5000 *Macromolecules* **2010**, *43*, 5000–5008
DOI: 10.1021/ma100304n

Macromolecules
ARTICLE

Isothermal Crystallization of Poly(L-lactide) Induced by Graphene Nanosheets and Carbon Nanotubes: A Comparative Study

Jia-Zhuang Xu,[†] Tao Chen,[‡] Chuan-Lu Yang,[§] Zhong-Ming Li,*[,†] Yi-Min Mao,[⊥] Bao-Qing Zeng,[‡] and Benjamin S. Hsiao[⊥]

[†]*College of Polymer Science and Engineering and State Key Laboratory of Polymer Materials Engineering, Sichuan University, Chengdu 610065, P. R. China,* [‡]*Vacuum Electronics National Laboratory, School of Physical Electronics, University of Electronic Science and Technology of China, Chengdu 610054, P. R. China,* [§]*Department of Physics and Electrons, Ludong University, Yantai 264026, P. R. China, and* [⊥]*Department of Chemistry, Stony Brook University, Stony Brook, New York 11794-3400*

Received February 7, 2010; Revised Manuscript Received April 22, 2010

ABSTRACT: Low-dimensional nanoparticles have a strong ability to induce the crystallization of polymer matrices. One-dimensional carbon nanotubes (CNTs) and two-dimensional graphene nanosheets (GNSs), both of which are both carbon-based nanoparticles, provide a good opportunity to investigate the effects of differently dimensional nanoparticles on the crystallization behavior of a polymer. For this purpose, respective nanocomposites of CNTs and GNSs with poly(L-lactide) (PLLA) as matrix were prepared by solution coagulation. Time-resolved Fourier-transform infrared spectroscopy (FTIR) and synchrotron wide-angle X-ray diffraction (WAXD) were performed to probe chain conformational changes and to determine the crystallization kinetics during the isothermal crystallization of the PLLA nanocomposites and neat PLLA, especially in the early stages. Both CNTs and GNSs could serve as nucleating agents in accelerating the crystallization kinetics of PLLA; however, the ability of CNTs to induce crystallization was stronger than that of GNSs. On increasing the content of CNTs from 0.05 to 0.1 wt %, the induction period was shortened and the crystallization rate was enhanced, but the reverse situation was found for GNSs nanocomposites. In the case of neat PLLA, $-CH_3$ interchain interactions preceded $-(COC + CH_3)$ interchain interactions during the crystallization. Conversely, in the CNTs and GNSs nanocomposites, the conformational ordering began with $-(COC + CH_3)$ interchain interactions, which resulted directly in a reduced induction period. Interchain interactions of this type could be explained in terms of surface-induced conformational order (SICO). Finally, the effect of the dimensionality of the nanoparticles on the crystallization behavior of PLLA is discussed.

Introduction

Carbon nanotubes (CNTs) have been extensively accepted as effective nucleating agents that facilitate the crystallization of various polymers. Not only are the crystallization temperatures and crystallization rates of semicrystalline polymers such as isotactic polypropylene, polyethylene, and poly(ethylene terephthalate) enhanced by the presence of CNTs, but amorphous polymers such as polycarbonate may also be induced to form a crystalline structure. The onset crystallization temperature of isotactic polypropylene containing 0.1 wt % CNTs was increased by about 9 °C from 122 °C for the neat polypropylene to 131 °C when crystallizing from the quiescent melt.[1] The half-crystallization time ($t_{1/2}$) of polyethylene loaded with 0.1 wt % CNTs was reduced to 7% of the value for neat polyethylene at 122 °C.[2] Even at a concentration as low as 0.03 wt %, the crystallization of poly(ethylene terephthalate) could also be accelerated by CNTs.[3] In a further example, the partially crystalline structure of polycarbonate, which is usually considered to be glassy, was observed in annealed polycarbonate/CNTs composites.[4] The effective nucleating ability of CNTs is generally attributed to their high specific surface areas and large aspect ratios.[1−5] CNTs may also induce a unique crystalline morphology; e.g., a so-called nanohybrid shish-kebab (NHSK) structure has been observed in the presence of CNTs, in which disk-shaped polymer single crystals as "kebabs" are patterned periodically on the surface of CNTs, which thus act as the "shish". Dilute solution formation, as proposed by Li et al., is a common method for preparing NHSK structures.[6−8] Recently, the NHSK structure has been observed in samples obtained by direct melt compounding in industrial polymer-processing equipment.[9] The formation mechanism of NHSK is considered as "soft epitaxy".[7,8]

In recent years, graphene nanosheets (GNSs), consisting of one- or several-atom-thick two-dimensional (2D) graphite layers, have attracted considerable attention.[10] It has been reported that GNSs have outstanding mechanical and electrical properties.[11,12] The in-plane Young's modulus of GNSs is about 1 TPa, comparable to those of CNTs (270−950 GPa), while its stress−strain behavior is very similar to that of CNTs, making it an ideal nanosized reinforcing and multifunctional filler for polymers.[13−17] By adding 0.1 wt % functionalized graphene sheets, the thermomechanical properties of poly(methyl methacrylate) (PMMA) were dramatically improved. The Young's modulus and ultimate strength of the composite were about 1.8 and 1.2 times larger than those of neat PMMA, rivaling those of PMMA/CNTs composites with the same filler content. Moreover, the glass transition temperature of PMMA containing only 0.05 wt % functionalized graphene sheets showed an unprecedented shift of nearly 30 °C.[16] Percolation in polystyrene/graphene composites occurred when the filler concentration was only 0.1 vol %, which is about 3 times lower than that reported for any other two-dimensional filler. The electrical properties of the composites are comparable to the best

---

*To whom correspondence should be addressed. E-mail: zmli@scu.edu.cn.

values specified in the literature for nanotube−polymer composites.[17] However, unlike that of CNTs, GNSs-induced polymer crystallization has not received any attention.

Structurally, GNSs and CNTs are made up of graphite layers, indicating that they have the same fundamental structural unit. The most significant difference is their morphology: GNSs have a two-dimensional flat area made up of one- or several-atom layers, while the main tube part of CNTs can be regarded as consisting of curled graphite layers with two half-fullerenes capping either end of the tube. Compared with the 2D nanoplate-like GNSs, CNTs may be viewed as one-dimensional (1D) nanolines. It has been well established that the crystallization behavior of a polymer may be greatly influenced by the topological structure of a heterogeneous nucleating agent. For instance, the degree of nanoclay exfoliation was found to have a great influence on the crystallization behavior of poly(L-lactide) (PLLA). The intercalated and exfoliated nanocomposites exhibited significantly faster bulk crystallization kinetics compared to that of the neat matrix, and the chain conformational changes during the crystallization process of the exfoliated nanocomposites were quite different from those of the intercalated nanocomposites or the neat matrix, which was rationalized in terms of non-nucleating behavior.[18] The unique morphological features of GNSs and CNTs inspired us to perform a comparative study on the influences of these differently dimensional nanoparticles on the crystallization behavior of polymers.

In our previous study, employing time-resolved Fourier-transform infrared spectroscopy (FTIR), we observed a distinct difference in the molecular chain conformational evolution of PLLA with and without CNTs during the early period of the overall crystallization process.[19] Owing to strong noncovalent interactions between PLLA chains and CNTs, PLLA crystallization could be induced and accelerated by CNTs, which acted as a template for chains to landscape. These results have aroused our curiosities, prompting us to ask the following questions. In the presence of the GNSs, how does the molecular chain conformation of PLLA develop in the early stage of crystallization? What is the induced crystallization mechanism of these two kinds of carbon-based nanosized fillers? How does the topological structure of the nanoparticles impact on the ability to induce polymer crystallization? With these questions in mind, we carried out the work described herein.

As nucleation agents, 2D GNSs prepared by a modified Hummers method, and 1D CNTs were incorporated into the polymer matrix for a comparative study of their crystallization-inducing abilities. PLLA was chosen to blend with the nanofillers. PLLA is an increasingly used biodegradable and biocompatible polymer with a relatively slow crystallization rate, making it possible to detect its structure change online by time-resolved spectroscopy. Furthermore, the crystallization behavior and crystal structure of pure PLLA have been extensively investigated and characterized by various analytical techniques, especially FTIR.[20−33]

The changes in the characteristic bands representing specific group vibrations detected by in situ FTIR can be related to crystalline and amorphous fractions of a polymer. By following the intensity and shape changes of the characteristic bands or peaks online, one can obtain detailed information on the conformational ordering and ensuing crystallization behavior of polymers, making it a powerful method for probing the crystallization process, in particular at the molecular level and in the early stages.[34−37] For example, Li et al. reported the flow-induced conformational order of supercooled isotactic polypropylene at temperature around its normal melting point.[37] After the cessation of shear, different trends in the intensity evolutions of long and short helical bands were observed, indicative of coupling between the coil−helix transition and intermolecular ordering. Moreover, the characteristic infrared peaks of pure PLLA have been extensively investigated and well-defined in the literature.[28−30] FTIR has been successfully used to study conformational order in the very early stages and later crystallization of PLLA, the results of which may help in interpreting the FTIR data of PLLA nanocomposite crystallization.[18,19,31−33]

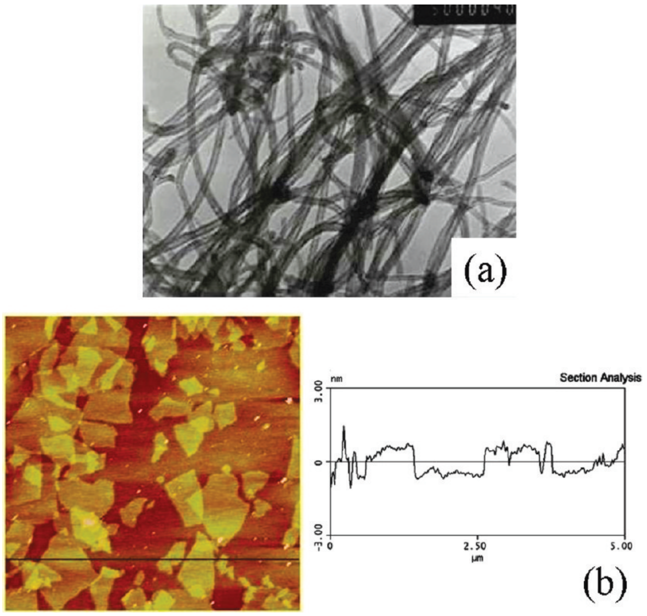

Figure 1. TEM image of CNTs (a) and AFM image of GNSs (b).

In this work, CNTs- and GNSs-induced isothermal crystallization of PLLA have been investigated by time-resolved FTIR and synchrotron wide-angle X-ray diffraction (WAXD) to compare the crystallization kinetics of PLLA induced by differently dimensional nanoparticles. We also discuss the mechanism of nucleation and growth of the PLLA nanocomposites. The results obtained are expected to help our understanding of the relationship between the structures and properties of polymer composites reinforced with these two differently dimensional nanoparticles.

Experimental Section

Materials. The PLLA (model 4060D) used in this study was an injection-grade granular material manufactured by Cargill Dow Co. (Japan). The M_n and M_w were 6.24×10^4 g mol^{-1} and 9.32×10^4 g mol^{-1}, respectively. Multiwalled carbon nanotubes of outer diameter (o.d.) 30−50 nm and length 10−20 μm were purchased from Chengdu Organic Chemicals Co., Ltd., the Chinese Academy of Sciences R&D Center for Carbon Nanotubes. A transmission electron microscopy (TEM) image of the CNTs is shown in Figure 1a (provided by the manufacturer). Graphene nanosheets were synthesized from expanded graphites by the modified "Hummers" method in this study (see the Supporting Information for details of the preparation process).[38] An atomic force microscopy (AFM) image of the graphene nanosheets is shown in Figure 1b. Anhydrous ethanol (AR grade) and dichloromethane (AR grade) were purchased from Chengdu Kelong Chemical Reagent Factory (China) and were used as received.

Preparation of PLLA Nanocomposites. Solution coagulation was utilized to prepare the PLLA nanocomposites. The CNTs and GNSs contents of each type of nanocomposite were 0.05 and 0.1 wt %, respectively. Taking the PLLA/0.1 wt % CNTs nanocomposite as an example, the detailed experimental procedure was as follows: 0.01 g of CNTs was added to 100 mL of C_2H_5OH, and the mixture was subjected to ultrasound for 40 min to obtain a uniform dispersion. At the same time, 10 g of PLLA was completely dissolved in 100 mL of CH_2Cl_2.

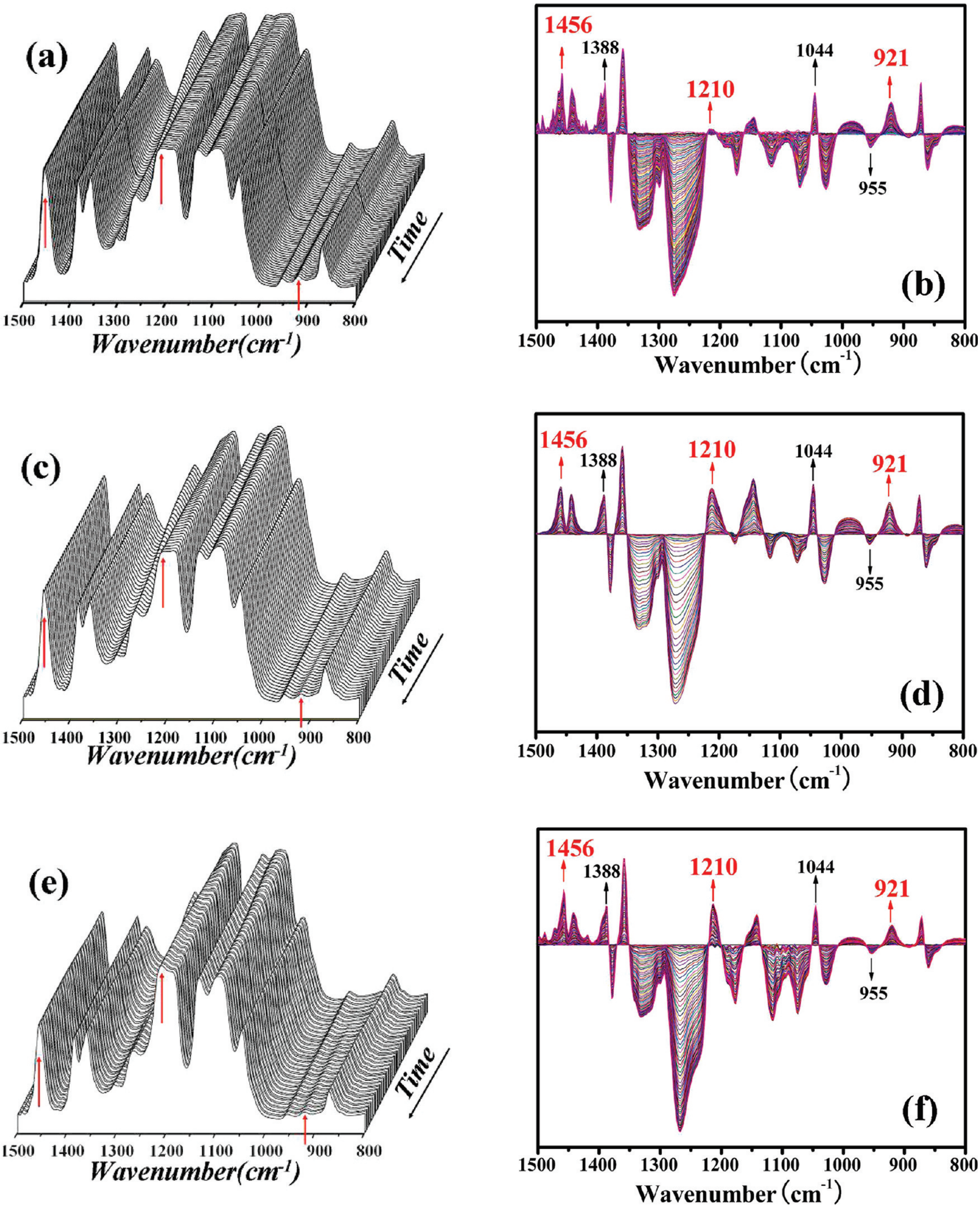

Figure 2. Time-resolved spectra and difference spectra in the range 1500−800 cm^{-1} of neat PLLA (a, b), PLLA/0.1 wt % CNTs (c, d), and PLLA/0.1 wt % GNSs (e, f) isothermally crystallizing at 124 °C.

By dropping the predispersed C_2H_5OH/CNTs suspension into the CH_2Cl_2/PLLA hybrid, coagulated material precipitated continuously. Thereafter, C_2H_5OH was poured into the mixture until no more coagulated material precipitated. The coagulates formed by the PLLA/CNTs nanocomposites were then transferred to evaporating dishes, left overnight at room temperature, and then dried in a vacuum oven for 1 day at 80 °C to evaporate the any residual solvent. Films of PLLA/CNTs nanocomposites were obtained by molding the coagulations at 180 °C for 10 min. Films of neat PLLA were prepared under the same conditions for comparison purposes.

Atomic Force Microscopy (AFM) Characterization. Images of GNSs were examined by a Nanoscope Multimode and Explore atomic force microscope (Vecco Instruments). Samples for AFM observation were prepared by depositing dispersions of GNSs in deionized water on a fresh Si substrate and allowing them to dry in air. Typical images were obtained at a line scan rate of 2 Hz and line scanning of 521 under ambient conditions.

Time-Resolved Fourier-Transform Infrared Spectroscopy (FTIR) Characterization. In situ IR spectra were collected over the wavenumber range 600−4000 cm^{-1} using a Bruker TENSOR 37 FTIR spectrometer with a DTGS detector in transmission mode. The spectra were obtained by averaging 16 scans at a resolution of 2 cm^{-1} with 1 min intervals. Background spectra used for reduction were collected at the same temperatures as those of the samples. A homemade parallel-plate cell controlled to within ±1 °C was employed as the hot stage. Two ZnSe plates were used as IR windows enclosing the membrane of PLLA nanocomposites. The samples were kept at 200 °C for 10 min to erase any thermal history and then cooled to the required crystallization temperature T_c (124 °C) in less than 2 min. When the temperature reached 124 °C, data collection was started and was continued until crystallization of the samples was complete. The baseline of each spectrum was linearly corrected according to the same standard, and the intensities of the characteristic bands were used to follow the conformational changes and crystallization kinetics for both PLLA nanocomposites and neat PLLA samples.

Synchrotron Wide-Angle X-ray Diffraction (WAXD) Characterization. Synchrotron WAXD was carried out using beamline X27C at the National Synchrotron Light Source, Brookhaven National Laboratory. The wavelength of the X-ray beam was 0.1371 nm. An MAR CCD detector (MAR-USA) with a resolution of 1024 × 1024 pixels (pixel size = 158 μm) was used to acquire data for wide-angle experiments. An Al_2O_3 (aluminum oxide) standard was used to calibrate the scattering angle for WAXD, and air scattering was subtracted. A Linkam CSS-450 high-temperature shear stage modified for in situ X-ray scattering measurements was employed to control the thermal history of samples to be the same as that in time-resolved FTIR. The 2θ angles of the samples were corrected by the function $q = 4\pi \sin \theta_1/\lambda_1 = 4\pi \sin \theta_2/\lambda_2$, where the first-order scattering vector, q, is a constant, and λ_1 (0.1371 nm) and λ_2 (0.1542 nm) are the representative wavelengths of the experimental beamline X27C and commonly used Cu Kα radiation, the Bragg angles of which corresponded to θ_1 and θ_2, respectively. The corrected 2θ angles of the 1D WAXD pattens shown below correspond to commonly used Cu Kα radiation in order to permit convenient comparison.

Results

Morphological Observation. In order to more easily understand the origin of the effects of the two differently dimensional nanoparticles on inducing polymer crystallization, it is necessary to compare their morphologies. Figure 1a shows a TEM micrograph of the CNTs used in this work. Their aspect ratio was more than 400, as estimated by dividing their length (10−20 μm) by the o.d. (30−50 nm), which allows the CNTs to be considered as one-dimensional nanolines with large surface curvature. Figure 1b shows an AFM image of the GNSs. It can be seen that the synthesized GNSs were only 1−2 nm thick, and their average calculated length was 0.87 μm with a large distribution. The GNSs consist of only 1−3 layers of graphite stacked in separate platelets, with the thickness of one layer being in the range 0.8−1.2 nm.[10−12,17] Not all GNSs are one-atom layers, but the lengths of the GNSs are nearly 3 orders of magnitude greater than their thicknesses, so the GNSs can be regarded as two-dimensional nanosheets with low surface curvature, in contrast to 1D CNTs. The 1D CNTs and 2D GNSs with totally different geometrical structures provide an important prerequisite for evaluating the effect of the dimensionality of the nanoparticles on polymer crystallization.

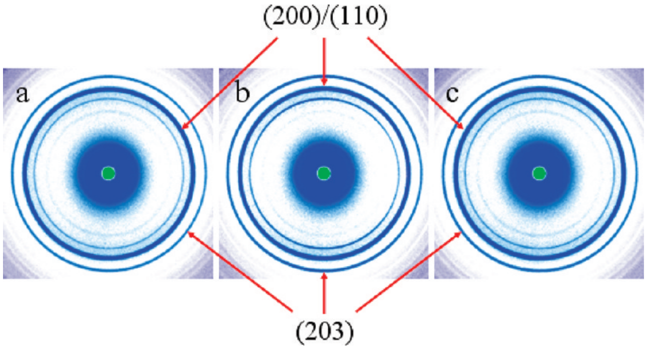

Figure 3. Representative 2D WAXD patterns of neat PLLA (a), PLLA/0.05 wt % CNTs (b), and PLLA/0.05 wt % GNSs (c) isothermally crystallizing at 124 °C, the selected times of which were 270, 40, and 60 min, respectively.

Monitoring of Isothermal Crystallization by in Situ FTIR Spectroscopy. Figure 2a,c,e shows the time dependence of the FTIR spectra of neat PLLA and its nanocomposites. The FTIR spectra are highly sensitive to structural changes during crystallization. The frequencies and the vibrational assignments for neat PLLA and its nanocomposites are based on values reported in the literature.[28−30] Intensity changes and band shifts of some significant characteristic peaks apparently occur with increasing crystallization time (Figure 2a,c,e). For instance, the intensity of the band at 1456 cm^{-1} increases, which indicates a change in the asymmetric deformation mode of CH_3 ($\delta_{as}(CH_3)$) and is representative of the $-CH_3$ interchain interaction. The peak at 1210 cm^{-1} is assigned to the C−O−C asymmetric vibration ($\upsilon_{as}(COC)$) linked to the asymmetric CH_3 rocking vibration ($\gamma_{as}(CH_3)$) and the most sensitive response to interchain conformational order, which shifts to higher wavenumbers with increased intensity and splits into two peaks at around 1210 and 1178 cm^{-1}. Moreover, the band at 921 cm^{-1} arising from the coupling of C−C backbone stretching and the CH_3 rocking mode is sensitive to the 10_3 helix chain conformation of PLLA α-crystals and is generally regarded as the crystalline peak. In the initial stages of the PLLA crystallization, the band at 921 cm^{-1} could not be observed, suggesting the absence of crystallites in the sample. With the increase of crystallization time, this peak became visible and its intensity gradually increased until the crystallization was complete. From the difference spectra (Figure 2b,d,f), the characteristic bands at 1456 and 921 cm^{-1} in the spectra of both nanocomposites and neat PLLA exhibit a discernible intensity change. However, the intensity of the band at 1210 cm^{-1} of the nanocomposites changes more obviously than that of the neat PLLA. It is strongly suggested that the interaction between C−O−C asymmetric vibrations and asymmetric CH_3 rocking vibrations is enhanced to a certain extent owing to the presence of CNTs and GNSs, which may be explained as discussed in the following. According to the literature,[18,19,31−33] the bands at 1456, 1210, and 921 cm^{-1} may be classified as crystalline-dependent peaks, all of which are in the positive region according to the difference spectrum obtained by subtracting the initial spectrum from the consecutive spectra as shown in Figure 2b,d,f. In the following discussion, the intensity changes of the characteristic bands at 1456 and 1210 cm^{-1}

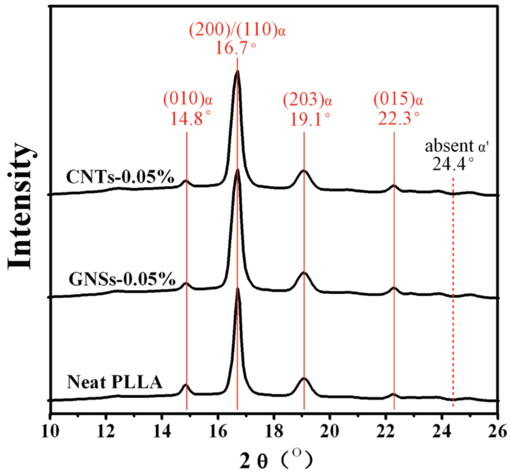

Figure 4. Representative 1D WAXD curves of neat PLLA, PLLA/0.05 wt % CNTs, and PLLA/0.05 wt % GNSs isothermally crystallizing at 124 °C, the selected times of which were 270, 40, and 60 min, respectively.

are used to probe the conformational changes in the backbone, while the 921 cm^{-1} band is adopted to investigate the diversification of the 10_3 helix and to compare the crystallization kinetics of the nanocomposites with that of neat PLLA.

Monitoring of Isothermal Crystallization by in Situ Synchrotron WAXD. To further investigate the formation and growth of PLLA crystals and to determine the crystal modification, synchrotron WAXD was employed to follow the isothermal crystallization of neat PLLA and its nanocomposites. Figure 3a−c illustrates representative 2D WAXD patterns at selected crystallization times. The strongest diffraction rings appearing at 16.7° and 19.1° represent (200)/(110) and (203) reflections of stable α-crystals. There is no evidence to suggest any orientation of PLLA crystallites in the PLLA/CNTs nanocomposites, suggesting isotropic distribution of the CNTs.[39,40]

Figure 4 shows 1D WAXD curves of neat PLLA and its nanocomposites at selected crystallization time corresponding to the 2D WAXD patterns shown in Figure 3. Besides the strongest diffraction rings appearing at 16.7° and 19.1°, some weak diffraction peaks at 14.8° and 22.3° indicative of (010) and (015) reflections of the α-form of PLLA are also observed, whereas the characteristic diffraction of PLLA α′-crystals at 24.4° could not be observed. This implies that no such crystals were present in any of the three systems; that is to say, the presence of CNTs and GNSs has no impact on the crystalline modification of the PLLA at this crystallization temperature.[33]

The evolution of the 1D WAXD profiles of neat PLLA and its nanocomposites during the initial 40 min of crystallization is shown in Figure 5. The 1D WAXD profiles always begin with the amorphous halo. With increasing isothermal crystallization time, the reflection peaks appear and gradually intensify, corresponding to the formation and growth of the PLLA crystals. The strongest and first visible diffraction in all three systems is at 16.7°, which is characteristic of the (200)/(110) reflection of the PLLA α-form. The starting times (t_α) for the appearance of the 16.7° diffraction peak could be observed directly from Figure 5a−c, which conform to the sequence (t_α(CNT) < t_α(GNS) < t_α(neat PLLA)), and the remaining weaker diffractions appear in the same order. This suggests that both CNTs and GNSs could serve as heterogeneous nucleation agents, shortening the induction period of crystallization of PLLA, but the nucleation ability of CNTs is stronger than that of GNSs.

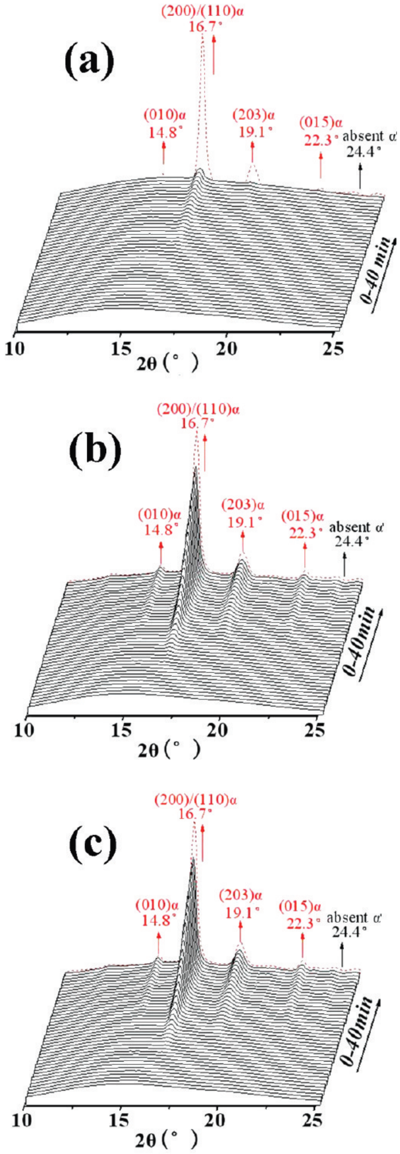

Figure 5. Initial 40 min evolution of the 1D WAXD profiles of neat PLLA (a), PLLA/0.05 wt % CNTs (b), and PLLA/0.05 wt % GNSs (c) shown by solid lines, where the last 1D WAXD cures are shown by red dotted lines, the selected times for which were 40 (a), 60 (b), and 270 min (c).

Isothermal Crystallization Kinetics. In situ FTIR nicely revealed the change in the crystalline band at 921 cm^{-1} arising from the coupling of C−C backbone stretching and the CH_3 rocking mode, which is sensitive to the 10_3 helix chain conformation of PLLA α-crystals. The absence of the band at 921 cm^{-1} in the early stages of the crystallization indicated that there were no crystallites in the melt. As the crystallization started, this peak became visible and its intensity increased until crystallization was complete (Figure 2a−c). In this study, the normalized height of the peak at 921 cm^{-1} was used to evaluate the kinetics of 10_3 helix formation, which represents the crystallization kinetics of PLLA, by means of the following equation:

$$X_{\mathrm{r}} = \frac{I_t - I_0}{I_\infty - I_0} \times 100\% \qquad (1)$$

where X_{r} is the relative crystallinity of PLLA, and I_0, I_t, and I_∞ are the intensities of the 921 cm^{-1} band at t_0, t, and t_∞, respectively. The same method has been adopted in previous literature.[18,19,31−33]

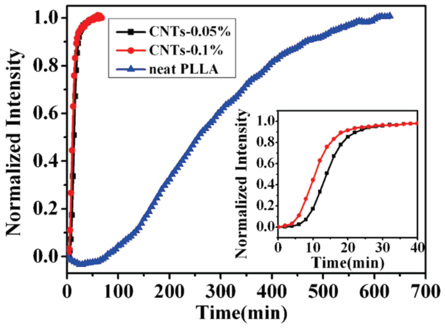

Figure 6. Normalized peak intensities at 921 cm^{-1} as a function of crystallization time for PLLA/0.05 wt % CNTs, PLLA/0.1 wt % CNTs, and neat PLLA.

Table 1. Induction Time (t_i) and Half-Crystallization Time ($t_{1/2}$) of PLLA Nanocomposites and Neat PLLA

	content of nanoparticles (wt %)	induction time, t_i (min)	half-crystallization time, $t_{1/2}$ (min)
PLLA/CNTs	0.05	10	15
	0.1	6	11
PLLA/GNSs	0.05	39	90
	0.1	84	173
neat PLLA		130	256

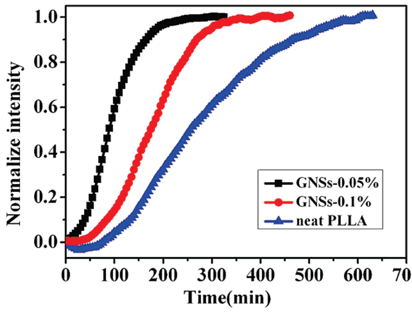

Figure 7. Normalized peak intensities at 921 cm^{-1} as a function of crystallization time for PLLA/0.05 wt % GNSs, PLLA/0.1 wt % GNSs, and neat PLLA. There is no need for an inset to distinguish the impact of the content of nanoparticles on the crystallization kinetics of PLLA.

Figure 6 shows the normalized intensity of the 921 cm^{-1} band as a function of time for neat PLLA and its CNTs nanocomposites at CNTs loadings of 0.05 and 0.1 wt %. The crystallization kinetics of these systems displays typical sigmoidal evolution. An induction period in the early stage is required, leading to an obvious increase in the conversion relative to the initial stage. The induction time t_i is defined as the time at which the normalized intensity reaches 1/10, and the half-crystallization time $t_{1/2}$ is defined as the time at which the crystallization reaches 50%. The values of t_i and $t_{1/2}$ correspond to the nucleation characteristics of the bulk PLLA and nanocomposite crystallization kinetics, respectively, which are summarized in Table 1. From Table 1, it can clearly be observed that t_i and $t_{1/2}$ for the PLLA/CNT nanocomposites (e.g., at 0.05 wt % CNTs, $t_i = 10$ min, $t_{1/2} = 15$ min) were far lower than those of neat PLLA ($t_i = 130$ min, $t_{1/2} = 256$ min), indicating the highly effective nucleation of the CNTs. As the CNTs content was increased from 0.05 to 0.1 wt %, $t_{1/2}$ of the nanocomposites further decreased from 15 to 11 min (see also the inset in Figure 6). It is suggested that with increasing CNTs content the greater number of nucleation sites provided by the CNTs would shorten the induction time and accelerate the rate of crystallization of PLLA.

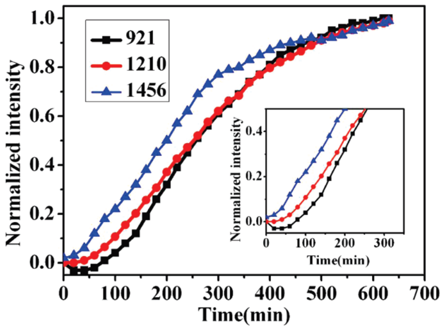

Figure 8. Normalized peak intensities at 921, 1210, and 1456 cm^{-1} as a function of crystallization time for neat PLLA during isothermal crystallization at 124 °C.

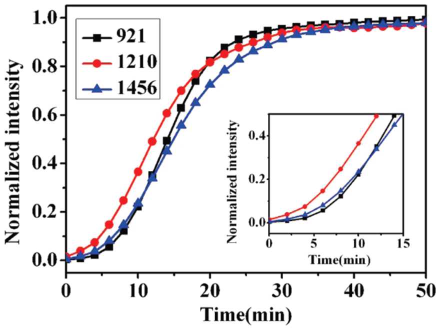

Figure 9. Normalized peak intensities at 921, 1210, and 1456 cm^{-1} as a function of crystallization time for PLLA/0.05 wt % CNTs during isothermal crystallization at 124 °C.

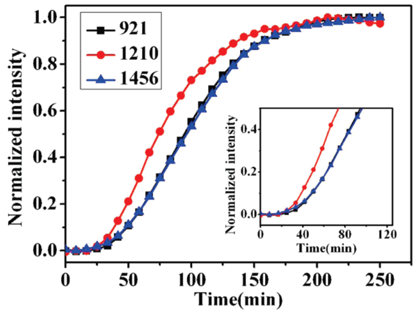

Figure 10. Normalized peak intensities at 921, 1210, and 1456 cm^{-1} as a function of crystallization time for PLLA/0.05 wt % GNSs during isothermal crystallization at 124 °C.

Plots of the normalized intensity of the 921 cm^{-1} band as a function of time for neat PLLA and its GNSs nanocomposites at GNSs contents of 0.05 and 0.1 wt % are shown in Figure 7. For the 0.05 wt % GNSs nanocomposite, the crystallization rate was strongly enhanced compared with that of the neat PLLA, indicating that GNSs also serve as nucleation agents for PLLA like CNTs. However, as shown in Table 1, t_i (39 min) and $t_{1/2}$ (90 min) of PLLA/0.05 wt % GNSs were obviously longer than those of PLLA/0.05 wt % CNTs ($t_i = 10$ min and $t_{1/2} = 15$ min). This implies that the induction ability of GNSs is weaker than that of CNTs. Unexpectedly, however, when the GNSs content reached 0.1 wt %, the crystallization kinetics of the nanocomposites was retarded. Presumably, the GNSs agglomerated in the PLLA nanocomposites at a high loading. The reasons for the differences in the induction abilities of CNTs and GNSs will be discussed in the next part.

Scheme 1. Schematic Diagrams of Conformational Ordering and Crystallization of PLLA in the Presence of CNTs (a−c) and GNSs (d−f)

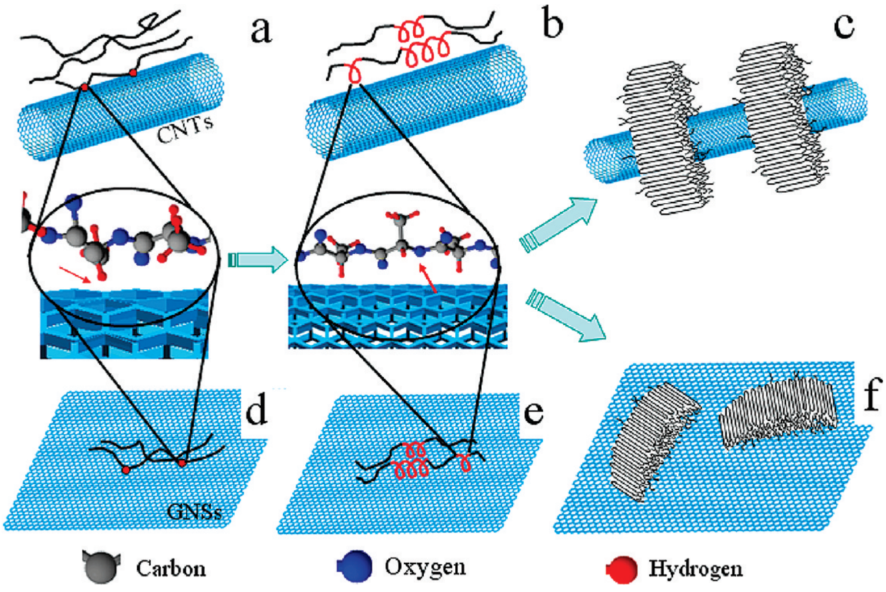

Discussion

It is necessary to discuss the mechanism of the 1D CNTs- and 2D GNSs-induced crystallization of PLLA in order to rationalize the varying abilities of these two differently dimensional nanoparticles to enhance PLLA crystallization. From the traditional crystallization point of view, the overall crystallization rate depends on two stages: nucleation and growth. Nucleation is the precondition for crystallization, and crystal growth involves the formation kinetics of a certain modification and growth space. In contrast to this view, Strobl proposed a multistage process to explain polymer crystallization. This idea shares the premise that the crystallization is preceded by an ordered precursor (so-called preordering).[41]

Therefore, molecular conformational order would also have a dramatic influence on the crystallization kinetics of the polymer.[34,42,43] For example, Zhu et al. reported that the partially ordered melt had a great impact on the crystallization behavior of isotactic polypropylene. With decreasing degree of order, the crystallization peak is shifted to a lower temperature and the exothermic enthalpy is increased.[34]

In the initial period of PLLA crystallization, how does the conformational order of the molecular chains change in the presence of differently dimensional nanoparticles? To clarify this issue, we followed the peak heights of the crystallinity band (10_3 helix formation) at 921 cm^{-1} and the regularity bands ($\delta_{as}(CH_3)$ and $\upsilon_{as}(COC) + \gamma_{as}(CH_3)$) at 1456 and 1210 cm^{-1} of the spectrum to investigate the nucleation mechanism of PLLA in the presence and absence of nanoparticles. The former crystallinity band reveals the intrachain interaction and the latter regularity bands represent the interchain interaction.[18,19] Here, eq 1 is again used to normalize the intensity change of the bands at 1456, 1210, and 921 cm^{-1}.

Figure 8 shows the normalized peak intensities at 921, 1210, and 1456 cm^{-1} as a function of crystallization time for neat PLLA during isothermal crystallization. The $\delta_{as}(CH_3)$ interchain interaction at 1456 cm^{-1} shows a fast change compared with the $\upsilon_{as}(COC) + \gamma_{as}(CH_3)$ interchain interaction at 1210 cm^{-1} and the 10_3 helix formation at 921 cm^{-1}. This indicates that the $-CH_3$ interchain interaction is a precondition for the formation of a stable PLLA helix structure.[18,32,33]

On the contrary, for the CNTs and GNSs nanocomposites, as shown in Figures 9 and 10, the change at 1210 cm^{-1}, which is representative of $\upsilon_{as}(COC) + \gamma_{as}(CH_3)$ and the most sensitive response to interchain conformational order, is detected considerably earlier than the changes in the other two bands at 1456 and 921 cm^{-1}. This clearly implies that CNTs and GNSs play an important role in the formation of the prepacking conformational ordering frame of PLLA. In our previous study, we found that CNTs could act as templates for the conformational ordering of PLLA chains, and surface-induced conformational order (SICO) was proposed.[19] A similar conclusion has also been reached in investigations of poly(butylene terephthalate)/CNTs and polyethylene/CNTs nanocomposites under both quiescent and shear conditions.[39,40] The order of the intensity changes of characteristic bands in the presence of CNTs and GNSs is the same: 1210 cm^{-1} > 1456 cm^{-1} ~ 921 cm^{-1}, suggesting that the induction mechanisms of CNTs and GNSs for PLLA crystallization are probably the same. Therefore, combining the above experimental results and the SICO mechanism, we propose the nucleation process of the carbon-based nanoparticles, CNTs and GNSs, in PLLA to be as follows. An initial contact between a PLLA chain and the CNTs or GNSs surface gives rise to the CH−π interaction, and successive −CH groups gradually attach themselves to the surface. This leads to partial or complete chain adsorption on the surface of CNTs and GNSs, as shown in Schemes 1a,d and their shared enlarged inset image. Later, there is interaction between C−O−C asymmetric vibrations and asymmetric CH_3 rocking vibrations ($\upsilon_{as}(COC) + \gamma_{as}(CH_3)$), whereupon the band at 1210 cm^{-1} appears, indicating that the conformers change from a random orientation to an in-plane one. Subsequently, PLLA backbones make contact with the preadsorbed ones through $-(COC + CH_3)$ interactions to form a unique conformationally ordered structure, which finally becomes the precursor of PLLA crystal growth, as depicted in Schemes 1b,e and their shared inset image. The existence of nanoparticles can be regarded as the landscape of the ordering of PLLA helices surrounding the PLLA/nanoparticles interface.

It has been reported that polymeric materials can form single crystals on the surfaces of CNTs and carbon nanofibers (CNFs), called the NHSK structure. For a larger diameter "shish" (i.e., CNFs), the "kebabs" showed multiple orientations, while for a small diameter "shish" (i.e., CNTs), the "kebabs" were perpendicular to the tube axis. Size-dependent soft epitaxy (SSE) was proposed by Li et al. to explain this special phenomenon, whereby epitaxial growth of polyethylene on CNTs and geometric confinement by the CNTs competing with each other determined by the surface curvature of the carbon-based nanofillers serve to control the chain orientation.[7] The most notable difference between CNTs and GNSs is their morphology. The surface curvature of GNSs tends to be infinitesimal and much less than that of CNTs under the actual conditions. Considering the mechanism of SSE, lattice matching should play a dominant role in surface-induced crystallization of GNSs with low surface curvature. PLLA chains adsorbed on the surface of GNSs need more time to adjust their conformations, making the induction process more complex. Indirect evidence for this was reported by Takenaka et al. They found that polyethylene crystallization on highly oriented pyrolitic graphite (HOPG) is indeed epitaxial and obeys the rules of lattice matching.[44] However, CNTs with large surface curvature can be viewed as rigid macromolecules, and thus geometric confinement becomes more significant. The PLLA chains might prefer to align along the tube axis, and strict lattice matching between the PLLA chains and the external graphitic sheet of CNTs is not required, simplifying the surface-induction process and shortening the induction period. Consequently, the induction period of CNTs nanocomposites is significantly shorter than that of GNSs nanocomposites, as observed from both the FTIR and WAXD results. As shown in Table 1, t_i (10 min) of PLLA/0.05 wt % CNTs is obviously shorter than that of PLLA/0.05 wt % CNTs ($t_i = 39$ min).

As regards the aspect of the growth space of PLLA crystals, the 1D CNTs could provide the whole space for PLLA crystallization around them, and only one nucleating site is needed for PLLA to form a disk-shaped single crystal on the surface of CNTs, as shown in Scheme 1c. However, unlike with the 1D CNTs, the growth spacing on the GNS surface might only be half of that on the CNTs surface, taking into account the considerable 2D flat area of GNSs. Meanwhile, due to lattice matching, the PLLA single crystals show multiple orientations, which might impinge on adjacent single crystals to suppress crystal growth. Hence, the crystallization rate of PLLA in the GNSs nanocomposite is slower than that in the presence of a similar CNTs content ($t_{1/2}$(CNTs) < $t_{1/2}$(GNSs)).

It is certainly doubtful that different crystal modifications of the PLLA formed could also influence the crystallization kinetics of PLLA. It has been reported that the α′- and α-crystals could be formed in the range 100−120 °C,[25,33] while the region would change in the presence of other fillers or polymers.[45] By comparing the representative 1D WAXD profiles in Figure 4, the presence of the characteristic peaks of α-crystals and the absence of those of α′-crystals demonstrate that there were only α-crystals in all three of the systems. Thus, we could conclude that at T_c = 124 °C the CNTs and GNSs could only induce PLLA to form α-crystals; that is, the difference in crystallization kinetics of the nanocomposites has no influence on the crystal modification of PLLA.

As discussed above, strong noncovalent binding between CNTs and GNSs and polymer main chains results in unique conformational ordering of PLLA nanocomposites. The surfaces of CNTs and GNSs provide templates for the PLLA chains to become suitably oriented, which is the reason why they show the strong ability to induce PLLA crystallization. Moreover, the crystallization behavior of PLLA is significantly influenced by the dimensionality of the CNTs and GNSs, which could be explained in terms of SSE, but the modification of the PLLA crystallites formed is not influenced by the nature of the nanoparticles.

Conclusions

The effects of differently dimensional nanoparticles on the crystallization behavior of PLLA have been thoroughly investigated, for which two kinds of carbon-based nanoparticles were used as respective fillers incorporated into PLLA. One kind of nanofiller was CNTs with a large aspect ratio, considered to be one-dimensional nanolines, while the other was GNSs prepared by modified Hummer's method, which are well exfoliated from expandable graphites and show a two-dimensional topological structure.

Both CNTs and GNSs could serve as heterogeneous nucleation agents, shortening the induction period of crystallization and accelerating the crystallization rate, but the induction ability of CNTs was found to be stronger than that of GNSs. As the content of CNTs was increased from 0.05 to 0.1 wt %, the induction period was shortened and the crystallization rate was enhanced, while the reverse situation was observed for GNS nanocomposites.

In the case of neat PLLA, the conformational ordering begins with $-CH_3$ interchain interactions during the crystallization. Conversely, strong noncovalent binding between nanoparticles and polymer main chains results in unique conformational ordering of the CNTs and GNSs nanocomposites. Moreover, $-(COC + CH_3)$ interchain interactions precede $-CH_3$ interchain interactions, which may be explained in terms of surface-induced conformational order (SICO). This indicates that the surfaces of CNTs and GNSs provide templates for PLLA chains to become suitably oriented, dramatically shortening the induction periods of their nanocomposites.

Considering the mechanism of size-dependent soft epitaxy (SSE), the dimensionality of the nanoparticles has a great influence on the crystallization behavior of PLLA. For 1D CNTs, the PLLA chains might prefer to align along their tube axis, and strict lattice matching between the PLLA chains and the external graphitic sheet of CNTs is not required, simplifying the surface-induction process and shortening the induction period. Besides, the 1D CNTs could provide the whole space for PLLA crystallization around them, and only one nucleating site is needed for PLLA to form disk-shaped single crystals on the surface of CNTs. For 2D GNSs, on the other hand, lattice matching should play the dominant role in surface-induced crystallization. PLLA chains adsorbed on the surface of GNSs need more time to adjust their conformations, making the induction process more complex. Meanwhile, taking into account the considerable 2D flat area of GNSs, the PLLA single crystals on the GNSs surface could show multiple orientations, which might impinge on adjacent single crystals and suppress the crystal growth. This might be responsible for the observed difference between CNTs and GNSs in inducing PLLA crystallization.

Acknowledgment. The authors are indebted to Dr. Lixia Rong and Jie Zhu from the Synchrotron Light Source, Brookhaven National Laboratory, for their help with the WAXD measurements. The Chinese team is grateful for financial support from the National Outstanding Youth Foundation of China (Grant 50925311), and the US team is grateful for financial support from the National Science Foundation of the US (DMR-0906512).

Supporting Information Available: Detailed preparation process of graphene nanosheets. This material is available free of charge via the Internet at http://pubs.acs.org.

References and Notes

(1) Lu, K. B.; Grossiord, N.; Koning, C. E.; Miltner, H. E.; van Mele, B.; Loos, J. *Macromolecules* **2008**, *41*, 8081–8085.
(2) Haggenmueller, R.; Fischer, J. E.; Winey, K. I. *Macromolecules* **2006**, *39*, 2964–2971.
(3) Anand, K. A.; Agarwal, U. S.; Joseph, R. *Polymer* **2006**, *47*, 3976–3980.
(4) Sung, Y. T.; Kum, C. K.; Lee, H. S.; Byon, N. S.; Yoon, H. G.; Kim, W. N. *Polymer* **2005**, *46*, 5656–5661.
(5) Moniruzzaman, M.; Winey, K. I. *Macromolecules* **2006**, *39*, 5194–5205.

(6) Li, C. Y.; Li, L. Y.; Cai, W. W.; Kodjie, S. L.; Tenneti, K. K. *Adv. Mater.* **2005**, *17*, 1198–1202.

(7) Li, L. Y.; Li, C. Y.; Ni, C. Y. *J. Am. Chem. Soc.* **2006**, *128*, 1692–1699.

(8) Li, L. Y.; Yang, Y.; Yang, G. L.; Chen, X. M.; Hsiao, B. S.; Chu, B.; Spanier, J. E.; Li, C. Y. *Nano Lett.* **2006**, *6*, 1007–1012.

(9) Yang, J. H.; Wang, C. Y.; Wang, K.; Zhang, Q.; Chen, F.; Du, R. N.; Fu, Q. *Macromolecules* **2009**, *42*, 7016–7023.

(10) Geim, A. K.; Novoselov, K. S. *Nat. Mater.* **2007**, *6*, 183–191.

(11) Novoselov, K. S.; Geim, A. K.; Morozov, S. V.; Jiang, D.; Zhang, Y.; Dubonos, S. V.; Crigorieva, I. V.; Firsov, A. A. *Science* **2004**, *306*, 666–669.

(12) Novoselov, K. S.; Geim, A. K.; Morozov, S. V.; Jiang, D.; Katsnelson, M. I.; Grigorieva1, I. V.; Dubonos, S. V.; Firsov, A. A. *Nature* **2005**, *438*, 197–200.

(13) Lee, C. G.; Wei, X. D.; Kysar, J. W.; Hone, J. *Science* **2008**, *321*, 385–388.

(14) Yu, M. F.; Lourie, O.; Dyer, M. J.; Moloni, K.; Kelly, T. F.; Ruoff, R. S. *Science* **2000**, *287*, 637–640.

(15) Treacy, M. M. J.; Ebbesen, T. W.; Gibson, J. M. *Nature* **1996**, *381*, 678–680.

(16) Ramanathan, T.; Abdala, A. A.; Stankovich, S.; Dikin, D. A.; Herrera-Alonso, M.; Piner, R. D.; Adamson, D. H.; Schniepp, H. C.; Chen, X.; Ruoff, R. S.; Nguyen, S. T.; Aksay, I. A.; Prud'Homme, R. K.; Brinson, L. C. *Nat. Nanotechnol.* **2008**, *3*, 327–331.

(17) Stankovich, S.; Dikin, D. A.; Dommett, G. H. B.; Kohlhaas, K. M.; Zimney, E. J.; Stach, E. A.; Piner, R. D.; Nguyen, S. T.; Ruoff, R. S. *Nature* **2006**, *442*, 282–286.

(18) Krikorian, V.; Pochan, D. J. *Macromolecules* **2005**, *38*, 6520–6527.

(19) Hu, X.; An, H. N.; Li, Z. M.; G, Y.; Li, L. B.; Yang, C. L. *Macromolecules* **2009**, *42*, 3215–3218.

(20) Meaurio, E.; Zuza, E.; López-Rodríguez, N.; Sarasua, J. R. *J. Phys. Chem. B* **2006**, *110*, 5790–5800.

(21) Pan, P. J.; Kai, W. H.; Zhu, B.; Dong, T.; Inoue, Y. *Macromolecules* **2007**, *40*, 6898–6905.

(22) Pan, P. J.; Liang, Z. C.; Zhu, B.; Dong, T.; Inoue, Y. *Macromolecules* **2008**, *41*, 8011–8019.

(23) Hu, Y.; Sato, H.; Zhang, J. M.; Noda, I.; Ozaki, Y. *Polymer* **2008**, *49*, 4204–4210.

(24) Sakai, F.; Nishikawa, K.; Inoue, Y.; Yazawa, K. *Macromolecules* **2009**, *42*, 8335–8342.

(25) Bouapao, L.; Tsuji, H.; Tashiro, K.; Zhang, J. M.; Hanesaka, M. *Polymer* **2009**, *50*, 4007–4017.

(26) Zhang, X. G.; Loo, L. S. *Macromolecules* **2009**, *42*, 5196–5207.

(27) Meaurio, E.; Zuza, E.; Sarasua, J. R. *Macromolecules* **2005**, *38*, 1207–1215.

(28) Kister, G.; Cassanas, G.; Vert, M. *Polymer* **1998**, *39*, 267–273.

(29) Kang, S. H.; Hsu, S. L.; Stidham, H. D.; Smith, P. B.; Leugers, M. A.; Yang, X. Z. *Macromolecules* **2001**, *34*, 4542–4548.

(30) Meaurio, E.; López-Rodríguez, N.; Sarasua, J. R. *Macromolecules* **2006**, *39*, 9291–9301.

(31) Zhang, J. M.; Tsuji, H.; Noda, I.; Ozaki, Y. *J. Phys. Chem. B* **2004**, *108*, 11514–11520.

(32) Zhang, J. M.; Tsuji, H.; Noda, I.; Ozaki, Y. *Macromolecules* **2004**, *37*, 6433–6439.

(33) Zhang, J. M.; Duan, Y. X.; Sato, H.; Tsuji, H.; Noda, I.; Yan, S. K.; Ozaki, Y. *Macromolecules* **2005**, *38*, 8012–8021.

(34) Zhu, X. Y.; Yan, D. Y.; Yao, H. X.; Zhu, P. F. *Macromol. Rapid Commun.* **2000**, *21*, 354–357.

(35) Zhu, X. Y.; Yan, D. Y.; Fang, Y. P. *J. Phys. Chem. B* **2001**, *105*, 12461–12463.

(36) An, H. N.; Zhao, B. J.; Ma, Z.; Shao, C. G.; Wang, X.; Fang, Y. P.; Li, L. B.; Li, Z. M. *Macromolecules* **2007**, *40*, 4740–4743.

(37) Geng, Y.; Wang, G. L.; Cong, Y. H.; Bai, L. G.; Li, L. B.; Yang, C. L. *Macromolecules* **2009**, *42*, 4751–4757.

(38) Hummers, W. S.; Offeman, R. E. *J. Am. Chem. Soc.* **1958**, *80*, 1339–1339.

(39) Haggenmueller, R.; Fischer, J. E.; Winey, K. I. *Macromolecules* **2006**, *39*, 2964–2971.

(40) García-Gutiérrez, M. C.; Hernández, J. J.; Nogales, A.; Panine, P.; Rueda, D. R.; Ezquerra, T. A. *Macromolecules* **2008**, *41*, 844–851.

(41) Strobl, G. *Prog. Polym. Sci.* **2006**, *31*, 398–442.

(42) Tanaka, F. *Macromolecules* **2000**, *33*, 4249–4263.

(43) Varshney, V.; Carri, G. A. *Macromolecules* **2005**, *38*, 780–787.

(44) Takenaka, Y.; Miyaji, H.; Hoshino, A.; Tracz, A.; Jeszka, J. K.; Kucinska, I. *Macromolecules* **2004**, *37*, 9667–9669.

(45) Pan, P. J.; Liang, Z. C.; Zhu, B.; Dong, T.; Inoue, Y. *Macromolecules* **2009**, *42*, 3374–3380.